

Polarized Rabi-coupled and spinor boson dropletsT. A. Yoğurt ^{1,*}, A. Keleş ¹ and M. Ö. Oktel ²¹*Department of Physics, Middle East Technical University, Ankara 06800, Turkey*²*Department of Physics, Bilkent University, Ankara 06800, Turkey*

(Received 17 October 2022; accepted 15 February 2023; published 27 February 2023)

Self-bound quantum droplets form when the mean-field tendency of the gas to collapse is stabilized by the effectively repulsive beyond-mean-field fluctuations. The beyond-mean-field effects depend on Rabi frequency ω_R and quadratic Zeeman effect q for the Rabi-coupled Bose mixtures and the spinor gases, respectively. For a quantum droplet, the effects of varying ω_R and q have recently been examined only for unpolarized Rabi-coupled Bose mixtures and unpolarized spinor gases. In this paper, we theoretically explore the stability of the droplet phase for polarized Rabi-coupled Bose mixtures and polarized spinor gases. We calculate the beyond-mean-field corrections for both gases with polarized order parameters and obtain the phase diagram of the droplets on the parameter space of Rabi frequency ω_R and detuning δ for Rabi-coupled mixtures and quadratic Zeeman energy q and linear Zeeman energy p for spinor gases. Finally, we highlight the similarities and differences between the two systems and discuss their experimental feasibility.

DOI: [10.1103/PhysRevA.107.023322](https://doi.org/10.1103/PhysRevA.107.023322)**I. INTRODUCTION**

Theoretical prediction and experimental realization of the bosonic droplets strikingly highlight the significance of the beyond-mean-field (BMF) effects which generally give minor corrections. Self-trapping of a Bose-Einstein condensate (BEC) that is otherwise collapsing is only possible if the BMF fluctuations are taken into account [1,2]. In a trapped single component BEC with attractive interactions, the mean-field (MF) interaction energy scales with $-N^2|a|/R^3$, where N is the number of particles, R is the radius of the condensate, and a is the s -wave scattering length ($a < 0$) [3]. The trapping potential $\propto NR^2$ and kinetic energy $\propto N/R^2$ of the condensate may balance this attractive MF interaction and yield a metastable BEC only if the particle number is below some maximum value [3]. The situation is drastically different in the case of self-bound droplets. There, the MF collapse is stabilized by the BMF quantum fluctuations even without a confining potential [1,2,4–16], and droplets exhibit a minimum particle number below which the gas is no longer stable [2]. As particle number N decreases, the kinetic energy eventually dominates and causes the gas to expand.

In addition to these constraints in the particle number, the stability of droplets also depends on the interaction parameters. Consider the three different classes of Bose droplets: dipolar [1], binary mixture [2], and spinor [16]. For the dipolar droplets, the dipole-dipole ϵ_{dd} and contact interactions a_s ; for binary mixtures, intraspecies a_{11} , a_{22} and interspecies a_{12} contact interactions; for spin-1 gas, the spin-zero channel a_0 and the spin-2 channel a_2 interactions are the fundamental interaction parameters to be considered. These parameters should be fine tuned to drive the MF energy of the system

towards collapse and balance the collapse with the BMF energy.

The leading theoretical tool to study quantum droplets is the Bogoliubov theory [1,2,16], which successfully captures the physics behind the droplet phase. However, there exists a quantitative disagreement between the theoretical prediction and experimental results for the critical number of particles [4,9,17]. Different proposals exist to resolve this disagreement such as higher-order contributions [18,19], bosonic pairing [20], beyond Born-approximation [21], or general Gaussian-state *Ansätze* [22]. In this paper, we use the Bogoliubov theory since it provides a sufficient qualitative understanding of the droplet phenomena. Furthermore, to be able to rely on the results of Bogoliubov theory, the gas should be in the dilute regime $\sqrt{na^3} \ll 1$, where n is the density of the condensate. Hence, the requirement of such stringent fine tuning motivates a search for additional probes to adjust droplet formation in cold atom experiments.

Recently, Bose mixtures with Rabi coupling between the hyperfine states of the particles attracted attention due to interesting many-body effects, such as effective tunable three-body interactions [8,23–25]. The coupling between the two levels of the system makes the BMF energy depend on the Rabi frequency ω_R [24] and provides an additional mechanism to tune the droplet density. Similar to a critical particle number, there is a critical Rabi frequency ω_c above which the droplet is no longer self-trapped [8]. For the spinor droplets, the quadratic Zeeman energy-dependent BMF correction of the spinor gas plays an analogous role with a maximum quadratic Zeeman energy q_c above which the droplet expands [16]. Additionally, when nonzero quadratic Zeeman energy or Rabi frequency is introduced, one of the gapless Bogoliubov modes becomes gapped for both spinor and Rabi-coupled mixtures. The MF energies can be controlled by the detuning δ for Rabi-coupled gases and linear Zeeman energy p for spinor

*ayogurt@metu.edu.tr

gases. These similarities prompt us to investigate their droplet states comparatively.

Previously, both the Rabi-coupled binary mixture droplets [8] and the spinor gas droplets [16] were studied for zero net polarization. For the Rabi-coupled droplets, the detuning δ is assumed to be zero, which yields an unpolarized ground-state order parameter within the MF picture. Similarly, for the spinor droplet [16], the MF ground states are studied with zero magnetization $\langle \mathbf{F} \rangle$. In this paper, we theoretically explore the droplet formation for the polarized Rabi-coupled binary mixture and the spin-1 gas. We examine how the nonzero polarization affects the MF and BMF energies and discuss the feasibility of the droplet phases under finite polarization. For the Rabi-coupled binary mixtures, the nonzero detuning δ leads to an asymmetry in the particle number of the two levels within the MF ground state. Finite polarization alters both the MF and BMF interaction energies. For a given Rabi frequency ω_R , there is a critical value of the detuning δ_c above which the droplet is not self-trapping. Similarly, for the spin-1 droplet, finite magnetization alters the MF and BMF interactions and a critical magnetization \tilde{p}_c exists for given quadratic Zeeman energy q . Using these critical values, we obtain the droplet phase boundary of the Rabi-coupled mixture and spinor gas in the ω_R - δ and q - p planes, respectively.

This paper is organized as follows. In Sec. II, we summarize the Bogoliubov theory of Rabi-coupled binary mixtures and discuss the possible MF ground states and mechanical stability of the mixture. In Sec. III, we develop the formulation of the polarized Rabi-coupled droplet and present our numerical results on the droplet phase boundary in the ω_R - δ plane. In Sec. IV, we summarize the Bogoliubov theory of polarized spin-1 gas and discuss the mean-field order parameters for antiferromagnetic interactions $c_1 > 0$. In Sec. V, we develop the formulation of the polarized spinor droplet and present the droplet phase boundary in the p - q plane. In Sec. VI, we discuss the experimental feasibility of the proposed phenomena and highlight the similarities and differences between the polarized Rabi-coupled and spinor droplets.

II. RABI-COUPLED BOSE MIXTURES: BOGOLIUBOV THEORY

We consider a BEC consisting of N atoms in two internal states, $m = 1, 2$ with the corresponding s -wave scattering lengths a_{11} , a_{22} , and a_{12} . The internal states are coupled through a Rabi frequency ω_R and detuning δ . Applying the rotating wave approximation to eliminate the explicit time dependence, the Hamiltonian of this Rabi-coupled binary mixture is given by [24]

$$\begin{aligned} \hat{H} = \int d\mathbf{x} \left\{ \sum_{m=1,2} \hat{\Psi}_m^\dagger(\mathbf{x}) \left(-\frac{\hbar^2 \nabla^2}{2M} \right) \hat{\Psi}_m(\mathbf{x}) \right. \\ + \sum_{m,m'} \left[\frac{g_{mm'}}{2} \hat{\Psi}_m^\dagger(\mathbf{x}) \hat{\Psi}_{m'}^\dagger(\mathbf{x}) \hat{\Psi}_{m'}(\mathbf{x}) \hat{\Psi}_m(\mathbf{x}) \right] \\ - \hbar\omega_R [\hat{\Psi}_1^\dagger(\mathbf{x}) \hat{\Psi}_2(\mathbf{x}) + \hat{\Psi}_2^\dagger(\mathbf{x}) \hat{\Psi}_1(\mathbf{x})] \\ \left. - \hbar \frac{\delta}{2} [\hat{\Psi}_2^\dagger(\mathbf{x}) \hat{\Psi}_2(\mathbf{x}) - \hat{\Psi}_1^\dagger(\mathbf{x}) \hat{\Psi}_1(\mathbf{x})] \right\} \quad (1) \end{aligned}$$

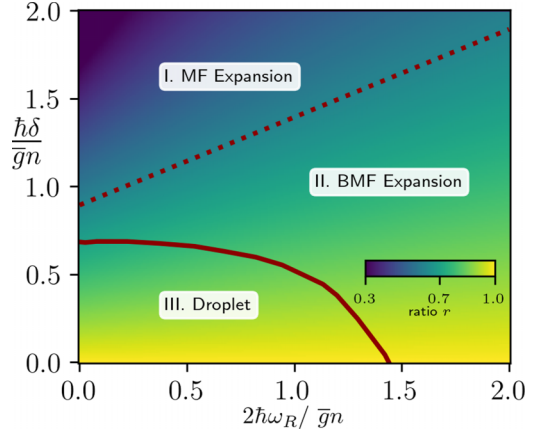


FIG. 1. The phase diagram of Rabi-coupled Bose mixture as a function of Rabi frequency $\frac{2\hbar\omega_R}{\bar{g}n}$ and detuning $\frac{\hbar\delta}{\bar{g}n}$ for $\frac{g_{12}}{g} < -1$, and $g > 0$. The shade (color bar) indicates the ratio $r = \sqrt{N_1/N_2}$ in the MF ground state (2). The dashed (red) line indicates the boundary above or below which the total MF two-particle interaction for $g_{12}/g = -1.5$ is repulsive or attractive, respectively. The solid (red) line is the boundary of the self-trapped droplet phase. In region I, the gas expands due to the repulsive MF interaction. In region II, the MF energy is attractive but the repulsive BMF energy is relatively strong to lead to the expansion. In region III, the MF attraction is stabilized by repulsive BMF energy to form a droplet.

where $g_{mm'} = 4\pi a_{mm'} \hbar^2/M$ is the coupling constant of the s -wave interaction among the atoms of mass M within the internal states m and m' . $\hat{\Psi}_m^\dagger(\mathbf{x})$ and $\hat{\Psi}_m(\mathbf{x})$ are the field operators that create and annihilate the particle with internal state m at position \mathbf{x} , respectively.

To understand the ground-state order parameter within the MF picture and how it differs from the binary mixture without Rabi coupling, we focus on the MF energy of the gas with an equal intraspecies scattering length $g_{11} = g_{22} = g$ for simplicity. The MF energy is given by [25,26] (see Appendix A for details)

$$\frac{E_{\text{MF}}}{N} = -\hbar\omega_R \sin \theta - \frac{\hbar\delta}{2} \cos \theta + \frac{gN}{2V} - \frac{\bar{g}N}{2V} \sin^2 \theta \quad (2)$$

where $\bar{g} = \frac{g-g_{12}}{2}$. The wave functions of the condensate components $(\psi_1 \ \psi_2) = \sqrt{n}(\sin \theta/2 \ \cos \theta/2)$ where $\theta \in [0, \pi]$ is the polar angle on the Bloch sphere. Assuming the total number of particles N fixed, the problem of determining the MF ground state becomes finding θ that minimizes the energy (2). The ground-state MF order parameter $r \equiv \sqrt{N_1/N_2} = \tan(\theta/2)$ for any g_{12}/g with $\delta = 0$ can be found in Ref. [8].

Here, we are interested in the parameter space for $\delta \neq 0$. Since our purpose is to examine the order parameters in which the system can collapse within the MF picture, we assume $g_{12}/g < -1$ and $g > 0$, which gives collapse without phase separation. This interval also yields $\bar{g} > 0$. The ratios between the particle numbers r within the MF ground state for various ω_R and δ values are shown in Fig. 1. Without any detuning, the MF energy is minimized by $\theta = \pi/2$ or $r = 1$ for any ω_R . This is exactly the order parameter to which Cappellaro *et al.* [8] restrict their droplet analysis. As detuning δ becomes nonzero, the MF ground state becomes polarized $r \neq 1$. The polarization becomes sharper, i.e., $r \rightarrow 0$ or $\theta \rightarrow 0$, as either

$\omega_R \rightarrow 0$ or $\delta \rightarrow \infty$. The order parameter $r = \tan(\theta/2)$, and $\theta \in [0, \pi/2]$ changes smoothly over the parameter space (see Fig. 1).

Now let us discuss how the two-body interaction part ($\frac{gN^2}{2V} - \frac{\bar{g}N^2}{2V} \sin^2 \theta$) of the MF energy (2) changes with the detuning δ . On the ω_R axis, the MF ground state yields $r = 1$ or $\theta = \pi/2$ which gives the two-body interaction $\propto (g - \bar{g})n^2 = (g + g_{12})n^2/2$, where $n = N/V$ is the density of the gas. Since $g_{12}/g < -1$, the density collapse is expected within the MF picture. However, on the δ axis, the MF ground state yields $r = 0$ or $\theta = 0$ for $\hbar\delta/\bar{g}n > 2$. Hence, the MF two-body interaction is $\propto gn^2$. Since $g > 0$, the gas expansion is expected within the MF picture. Note that as detuning δ is increased from zero to infinity, the gas becomes more polarized. As the polarization of the gas increases, i.e., $r \rightarrow 0$, the effective MF interaction first becomes less attractive and then acts repulsive. Consequently, we expect a value of $\theta = \sin^{-1} \sqrt{g/\bar{g}}$, below which the MF interaction is repulsive. For $g_{12}/g = -1.5$, the line that separates this attractive and repulsive MF interaction is shown with the dashed red line in Fig. 1. For region I in Fig. 1, the MF energy is repulsive and favors an expansion of the gas. For regions II and III in Fig. 1, the MF energy is attractive.

Below, the free parameters of the Rabi-coupled mixture are taken as ω_R , r , g_{12} , g , and N . Furthermore, dimensionless parameters $\tilde{\omega} = \frac{\hbar\omega_R}{gn}$ and $\gamma = g_{12}/g$ are used when appropriate. The results are presented as functions of the parameter set $(\tilde{\omega}, r)$ which then can be mapped to the parameter plane (ω_R, δ) when necessary.

We calculate the BMF energy of each corresponding Bogoliubov mode separately using $E_{\text{BMF}}^{\pm} = \frac{1}{2} \sum_{\mathbf{k}} (E_{\mathbf{k}}^{\pm} - \lim_{\mathbf{k} \rightarrow \infty} E_{\mathbf{k}}^{\pm})$, where $E_{\mathbf{k}}^{\pm}$ are the Bogoliubov dispersions and we obtain (see Appendix A for details)

$$\frac{E_{\text{BMF}}^{\pm}}{V} = \alpha (gn)^{5/2} I_{\pm}(\tilde{\omega}, \gamma, r) \quad (3)$$

where $\alpha = \frac{M^{3/2}}{\sqrt{2\pi^2 \hbar^3}}$. See Appendix A for $I_{\pm}(\tilde{\omega}, \gamma, r)$. In the limit $\tilde{\omega} \rightarrow 0$ and $r = 1$, (3) recovers the BMF energy of the Bose mixture without Rabi coupling. In the limit $r \rightarrow 1$ for any $\tilde{\omega}$, the E_{BMF}^{\pm} expressions of Cappellaro *et al.* [8] are recovered for both modes. For more general cases ($r \neq 1$), we calculate the I_{\pm} numerically for various r values. For any $r \in [0.6, 1]$, where the MF energy is attractive when $\gamma = -1.5$, BMF energy (3) increases as either $\tilde{\omega}$ or ratio r increases, since I_{\pm} is a monotonically increasing function of both variables.

III. RABI-COUPLED BOSE MIXTURE DROPLET

We now discuss the possibility of self-trapping and neglect the ‘‘soft’’ Bogoliubov mode contribution $E_{\mathbf{k}}^{-}$, as in Refs. [2,11,16]. We first consider the infinite, homogeneous Rabi-coupled Bose mixture. The pressure of the gas is calculated from $P = -\partial(E_{\text{MF}} + E_{\text{BMF}}^+)/\partial V$ as follows:

$$P = \frac{g(1+r^4) + 2g_{12}r^2}{2(r^2+1)^2} n^2 + \alpha (gn)^{5/2} f(\tilde{\omega}) \quad (4)$$

where $f(\tilde{\omega}) = \frac{3}{2} I_{+}(\tilde{\omega}) - \tilde{\omega} I'_{+}(\tilde{\omega})$. For any g_{12}/g , there is a value of $r \in [0, 1]$ above which the pressure due to the MF energy is negative. Furthermore, this negative pressure can be

stabilized by a positive contribution from BMF energy, since $g > 0$ and $f(\tilde{\omega})$ is positive for any value of $\tilde{\omega}$. Under these circumstances, the vanishing pressure $P = 0$ condition can be reached. We obtain an implicit equation for the equilibrium density:

$$n_0 = \frac{[g(1+r^4) + 2g_{12}r^2]^2}{4(r^2+1)^4 \alpha^2 g^5 f^2(\tilde{\omega}_0)} \quad (5)$$

where $\tilde{\omega}_0 = \frac{\hbar\omega_R}{gn_0}$. If $\omega_R = 0$ and $r = 1$, this equilibrium density becomes $n_0^{(1)} = \frac{25|\delta g|^2}{16\alpha^2 g^5 (1+|\gamma|)^5}$, where $\delta g \equiv g_{12} + g$. Here, $n_0^{(1)}$ also approximates the density of the finite droplets in which the kinetic energy is negligible. As the Rabi frequency $\tilde{\omega}$ is increased for a fixed ratio r , the function $f(\tilde{\omega})$ and BMF energy become greater, which in turn decreases the equilibrium density of the droplet.

We study the feasibility of the finite droplet more quantitatively by obtaining the governing Gross-Pitaevskii equation (GPE). We use the locked-in approximation, i.e., different components of the droplet are in phase within any region and the density ratio of the components is fixed throughout the condensate. Therefore, a single scalar wave function is sufficient to represent both components. Hence, we assume a droplet wave function $\Psi(\mathbf{r}) = \psi(\mathbf{r})(\tau_1 \tau_2)^T$, where $\tau_1/\tau_2 = r$ and $|\tau_1|^2 + |\tau_2|^2 = 1$. We express the energy functional of the droplet using $n(\mathbf{r}) = |\Psi(\mathbf{r})|^2$ as

$$\begin{aligned} \mathcal{E}[\psi^*, \psi] &= \frac{\hbar^2}{2M} |\nabla \psi|^2 + \left(-\frac{2\hbar\omega_R r}{r^2+1} - \frac{\hbar\delta(1-r^2)}{2(1+r^2)} \right) |\psi|^2 \\ &+ \left(\frac{g}{2} - \frac{2\bar{g}r^2}{(1+r^2)^2} \right) |\psi|^4 \\ &+ \alpha g^{5/2} I_{+} \left(\frac{\hbar\omega_R}{g|\psi|^2}, \gamma, r \right) |\psi|^5 \end{aligned} \quad (6)$$

and write the wave function in dimensionless form $\psi(\mathbf{r}) = \sqrt{n_0^{(1)}} \phi(\mathbf{r})$. We minimize the total energy in the grand canonical ensemble $E = \int d^3\mathbf{r} \mathcal{E}[\psi^*, \psi] - \mu N$ where the chemical potential is fixed by the total number of particles $N = \int d^3\mathbf{r} |\psi|^2$. The resulting modified GPE is given by

$$\begin{aligned} \tilde{\mu} \phi &= -\frac{1}{8} \left(r + \frac{1}{r} \right)^2 \tilde{\nabla}^2 \phi + \left[2\alpha_4 |\phi|^2 + \frac{5\alpha_5}{2} I_{+} \left(\frac{\tilde{\omega}_0^{(1)}}{|\phi|^2}, r, \gamma \right) \right] |\phi|^3 \\ &- \alpha_5 \tilde{\omega}_0^{(1)} I'_{+} \left(\frac{\tilde{\omega}_0^{(1)}}{|\phi|^2}, r, \gamma \right) |\phi| \end{aligned} \quad (7)$$

where $\tilde{\omega}_0^{(1)} = \frac{\hbar\omega_R}{gn_0^{(1)}}$, $\alpha_4 = \frac{3}{2|\delta g|} \left(\frac{(r^2+1)^2 g}{2r^2} - 2\bar{g} \right)$, and $\alpha_5 = \frac{15}{8(1+|\gamma|)^{5/2}} \left(r + \frac{1}{r} \right)^2$. Equation (7) is written in the dimensionless form $\tilde{\mathbf{r}} = \mathbf{r}/\xi$, where $\xi = \sqrt{\frac{6\hbar^2}{M|\delta g|n_0^{(1)}}}$ is the coherence length of the droplet and the total particle number is scaled by $\tilde{N} = N/n_0^{(1)} \xi^3$. This modified GPE reduces to the form obtained by Petrov [2] when $\omega_R = 0$ and $r = 1$, since $\alpha_4 = -3/2$ and $\alpha_5 I_{+}(0, 1, \gamma) = 1$ in this limit. Below, we fix the scattering length ratio $\gamma = -1.5$, as in Cappellaro *et al.* [8].

We numerically solve the modified GPE (7) by imaginary time evolution and obtain the ground-state wave function. For

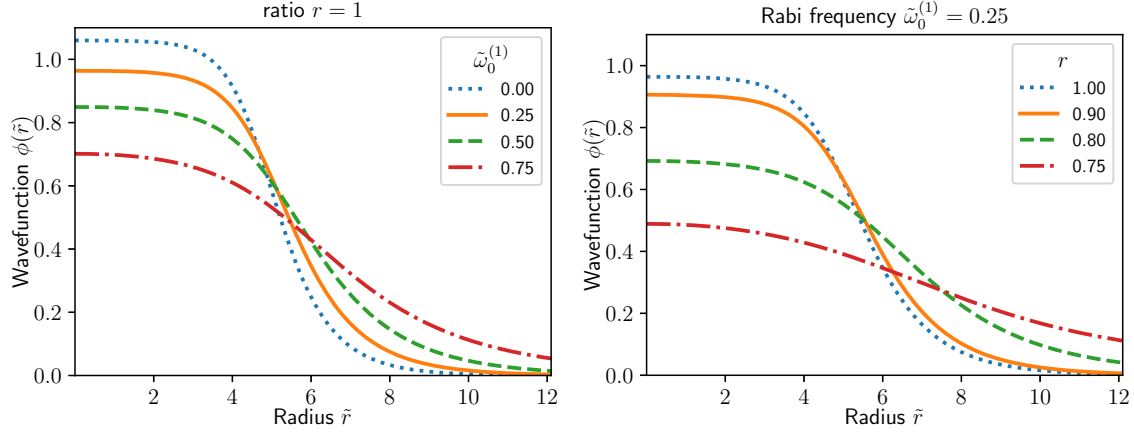


FIG. 2. The ground-state wave functions of the Rabi-coupled Bose mixture in the droplet phase for various values of $\tilde{\omega}_0^{(1)}$ and ratio r . Left: The wave functions for $\delta = 0$, i.e., $r = 1$ and different values of $\tilde{\omega}_0^{(1)}$. The above $\tilde{\omega}_c$ droplet is no longer self-trapped. Right: The wave functions for fixed $\tilde{\omega}_0^{(1)} = 0.25$ and varying ratio r , which shows the self-bound droplet until a critical value of $r_c \approx 0.7$. The total particle number $\tilde{N} = 500$ for both plots.

a fixed total particle number $\tilde{N} = 500$, we find the critical value of $\tilde{\omega}_0^{(1)}$ above which the droplet expands to infinity. One can expect that driving the gas to region II in Fig. 1, in which the MF energy is attractive, results in the collapse of the gas. However, the repulsion due to the BMF energy is strong enough to lead to an expansion. To understand this intuitively, consider a condensate with particle number \tilde{N} and radius \tilde{R} . The total energy \tilde{E} consists of attractive MF energy $\propto -\tilde{N}^2/\tilde{R}^3$, repulsive BMF energy $\propto I_+ \tilde{N}^{5/2}/\tilde{R}^{9/2}$, and the kinetic energy $\propto \tilde{N}/\tilde{R}^2$. For fixed \tilde{N} , as the BMF energy increases with greater I_+ , the equilibrium radius \tilde{R} of the droplet increases. Then the kinetic energy ($\propto \tilde{R}^{-2}$) becomes significant relative to both MF ($\propto \tilde{R}^{-3}$) and BMF ($\propto \tilde{R}^{-9/2}$) energies. Hence, the minimum of $\tilde{E}(\tilde{R})$ first shifts to greater \tilde{R} , and then disappears. For $\tilde{N} = 500$ and $\delta = 0$, or $r = 1$, the critical frequency is $\tilde{\omega}_c = 0.9$, above which the gas expands. Figure 2 shows the increase in the droplet radius with increasing $\tilde{\omega}_0^{(1)}$ up to the critical $\tilde{\omega}_c$ in the left panel.

As r decreases, the MF interaction energy [α_4 term in (2)] first decreases, then acts repulsive for $r < 0.62$. BMF energy (3) also decreases with r . However, since MF energy shrinks at a higher rate, we expect $\tilde{\omega}_c$ to become smaller with decreasing r . As r changes from 1 to 0.7, $\tilde{\omega}_c$ changes from 0.9 to 0, and we do not observe a droplet phase below $r = 0.7$. For $0.62 < r < 0.70$, the MF interaction of the gas is attractive. However, the MF energy is comparatively weak, hence any BMF repulsion leads to an expansion. We show the droplet wave function for various ratio r for fixed $\tilde{N} = 500$ and $\tilde{\omega}_0^{(1)} = 0.25$ in the right panel of Fig. 2.

We numerically obtain the critical $\tilde{\omega}_c$ values for different r and fixed $\tilde{N} = 500$ and $|\gamma| = 1.5$ to obtain the boundary of the droplet phase as shown in Fig. 1.

IV. SPIN-1 GASES: BOGOLIUBOV THEORY

In previous work [16], we study the spin-1 gas with vanishing magnetization (\mathbf{F}) = 0 and find that the spinor droplet is possible in the polar and antiferromagnetic phases if density interaction is negative $c_0 < 0$ and spin interaction is positive $c_1 > 0$. The quadratic Zeeman energy q in spinor gas is anal-

ogous to the Rabi frequency ω_R in Bose mixtures and both can tune the density of the droplet. As q increases, the BMF energy causes the droplet to expand and beyond a critical level of q the gas cannot self-bind. Similarly, the detuning δ in the Rabi-coupled mixture is analogous to the linear Zeeman shift p in the spinor gas.

Here, we extend our spinor droplet discussion to include the effects of nonzero magnetization $p \neq 0$. The ground-state order parameter changes only for the antiferromagnetic phase (see Fig. 3) and it gives a constant shift in the MF energy for the polar phase [27–29].

The spin-1 BEC with s -wave interactions and a uniform magnetic field along the z axis is described by the following Hamiltonian:

$$\hat{H} = \int d\mathbf{x} \left\{ \hat{\Psi}_m^\dagger(\mathbf{x}) \left(-\frac{\hbar^2 \nabla^2}{2M} + qm^2 - pm \right) \hat{\Psi}_m(\mathbf{x}) + \frac{c_0}{2} \hat{\Psi}_m^\dagger(\mathbf{x}) \hat{\Psi}_{m'}^\dagger(\mathbf{x}) \hat{\Psi}_{m'}(\mathbf{x}) \hat{\Psi}_m(\mathbf{x}) + \frac{c_1}{2} \hat{\Psi}_m^\dagger(\mathbf{x}) \hat{\Psi}_{m'}^\dagger(\mathbf{x}) \mathbf{F}_{mm'} \cdot \mathbf{F}_{m'n'} \hat{\Psi}_{n'}(\mathbf{x}) \hat{\Psi}_n(\mathbf{x}) \right\} \quad (8)$$

where $\hat{\Psi}_m^\dagger(\mathbf{x})$ and $\hat{\Psi}_m(\mathbf{x})$ create and annihilate the spin-1 atom in the magnetic quantum state $m = -1, 0, 1$, $\mathbf{F}_{mm'} = (F_{mm'}^x, F_{mm'}^y, F_{mm'}^z)$ are the spin-1 matrices in the z -axis basis, and the summation convention is used for m indices. The linear Zeeman energy $p = -g_L \mu_B B$ is the product of the Landé g_L factor, the Bohr magneton μ_B , and the applied magnetic field B . The quadratic Zeeman energy $q = q_B + q_{MW}$ can be tuned using both an external static field $q_B = \frac{(g_L \mu_B B)^2}{\Delta E_{hf}}$ and microwave field q_{MW} . Hence, the linear Zeeman energy p can be set using the static magnetic field B , whereas the quadratic Zeeman energy q can be independently tuned by the microwave fields [28]. Interactions in the density and spin channels are parametrized by coupling constants $c_0 = \frac{g_0 + 2g_2}{3}$ and $c_1 = \frac{g_2 - g_0}{3}$, where g_0 and g_2 are the total spin-zero and spin-2 channel coupling constants, respectively.

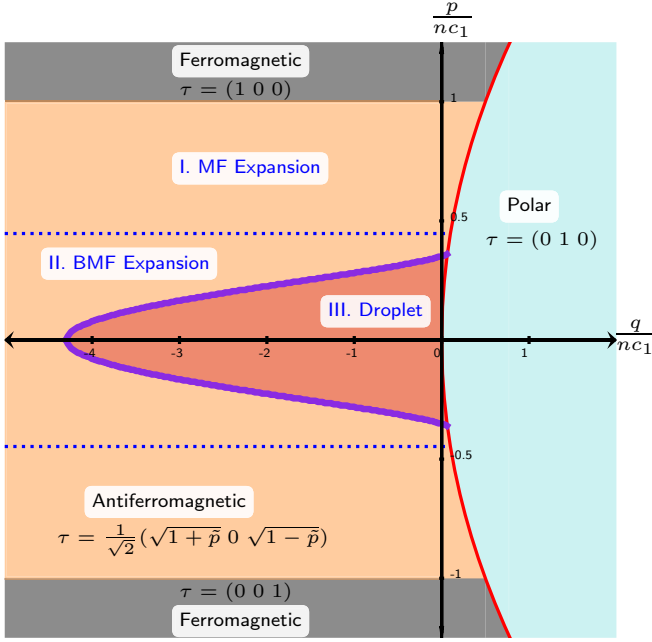


FIG. 3. The phase diagram of spin-1 gas as a function of quadratic q/nc_1 and linear p/nc_1 Zeeman energies. The orange region corresponds to the antiferromagnetic order $\tau^{\text{AF}} = 1/\sqrt{2}(\sqrt{1+\tilde{p}} \ 0 \ \sqrt{1-\tilde{p}})$. MF interaction is repulsive outside the dashed (blue) lines $|\tilde{p}| > 0.44$, and attractive inside $|\tilde{p}| < 0.44$ for $c_1/c_0 = -5$ with $c_0 < 0$. The droplet phase boundary is shown with solid (purple) line where the gas can be stabilized by BMF fluctuations. In region I, the repulsive MF interaction causes an expansion. In region II, while the MF energy is attractive, the BMF repulsion is relatively strong, leading to expansion. In region III, the MF attraction is stabilized by the repulsive BMF energy. The total particle number $\tilde{N} = 500$.

The MF ground-state order parameter τ is determined by minimizing the MF energy [28] (see Appendix B for derivation):

$$\frac{E_{\text{MF}}}{V} = \frac{n^2}{2}(c_0 + c_1 \langle \mathbf{F}^2 \rangle) + qn \langle F_z^2 \rangle - pn \langle F_z \rangle. \quad (9)$$

We consider the magnetic orders when the spin coupling constant is positive $c_1 > 0$ as shown in Fig. 3. For $p = 0$, the order parameter is $\tau_{\text{P}} = (0 \ 1 \ 0)$ if $q > 0$, or $\tau_{\text{AF}} = 1/\sqrt{2}(1 \ 0 \ 1)$ if $q < 0$. When $q > 0$, introducing nonzero p does not make any difference in τ_{P} around the q axis. However, if $q < 0$, the MF energy is minimized by a p dependent order parameter $\tau_{\text{AF}} = 1/\sqrt{2}(\sqrt{1+\tilde{p}} \ 0 \ \sqrt{1-\tilde{p}})$, where $\tilde{p} \equiv p/nc_1$. Note that $\langle F_z \rangle = \tilde{p}$, hence, τ_{AF} is defined for $-1 \leq \tilde{p} \leq 1$. Outside this interval, the order parameter becomes ferromagnetic. In this paper, we focus on this \tilde{p} dependent τ_{AF} to analyze how the spinor droplets in the antiferromagnetic phase are affected when the nonzero magnetization \tilde{p} is introduced.

The order parameter τ_{AF} gives $\langle F_z^2 \rangle = 1$, $\langle F_z \rangle = \tilde{p}$, and $\langle \mathbf{F} \rangle = \tilde{p} \hat{z}$ and the resulting MF and BMF energies are (see Appendix B for the derivation)

$$\frac{E_{\text{MF}}}{V} = (q - \tilde{p}p)n + \frac{(c_0 + c_1 \tilde{p}^2)n^2}{2}, \quad (10)$$

$$\begin{aligned} \frac{E_{\text{BMF}}}{V} &= \frac{8\sqrt{2}}{15} \alpha (c_1 n)^{5/2} I_0(\tilde{q}, \beta) \\ &+ \frac{8\sqrt{2}}{15} \alpha [(c_0 + c_1)n]^{5/2} [I_+(\kappa) + I_-(\kappa)] \end{aligned} \quad (11)$$

where $\tilde{q} = \frac{q}{nc_1}$, $I_{\pm} = \frac{(1 \pm \kappa)^{5/2}}{4\sqrt{2}}$, $\kappa \equiv \sqrt{1 - \frac{4\beta^2 c_0 c_1}{(c_0 + c_1)^2}}$, $\beta = \sqrt{1 - \tilde{p}^2}$, and $I_0(\tilde{q}, \beta)$ can be approximated as (see Appendix C)

$$I_0(\tilde{q}, \beta) \approx \frac{15\pi\beta^2}{32\sqrt{2}} \left[\sqrt{-\tilde{q} + 1} - \frac{\beta^2}{32} \frac{1}{(-\tilde{q} + 1)^{3/2}} \right]. \quad (12)$$

These expressions reproduce the results given in Ref. [16] for $\tilde{p} = 0$ and $\tau_{\text{AF}} = 1/\sqrt{2}(1 \ 0 \ 1)$.

Notice that when $\tilde{p} = 0$, the MF interaction is attractive if $c_0 < 0$. Interestingly, MF energy decreases in magnitude as polarization $|\tilde{p}|$ increases, and if $\tilde{p} > \sqrt{|c_0|/c_1}$, it becomes repulsive, which leads to an expansion of the gas above a critical level shown with dotted lines in Fig. 3.

In the attractive MF regime $\tilde{p} < \sqrt{|c_0|/c_1}$, the contribution of the BMF energy is repulsive since $c_1 > 0$, and it can stabilize the gas. The hard modes given above by I_+ and I_0 dispersion provide such stabilization whereas the soft mode I_- containing imaginary parts can be neglected, similar to the approach in the previous Sec. II and droplet studies [2,16].

V. POLARIZED AF SPIN-1 DROPLET

In the parameter regime $c_0 < 0$ and $c_1 > 0$, the pressure of the gas is calculated using the thermodynamic identity $P = -\partial E / \partial V$ with the total energy given by $E = E_{\text{MF}} + E_{\text{BMF}}^+ + E_{\text{BMF}}^0$, which gives

$$P = \left(\frac{c_0 + \tilde{p}^2 c_1}{2} \right) n^2 + \frac{4\sqrt{2}}{15} \alpha (c_1 n)^{5/2} h(\tilde{q}, \beta) \quad (13)$$

where $h(\tilde{q}, \beta) = 3I_0(\tilde{q}, \beta) + 3(c_0/c_1 + 1)^{5/2} I_+(\kappa) - 2\tilde{q} I_0'(\tilde{q}, \beta)$. Here, the prime on I_0 denotes the partial derivative with respect to \tilde{q} . The equilibrium density for the infinite homogeneous droplet can be found from the vanishing pressure

$$n_0 = \frac{225}{128} \frac{(c_0 + \tilde{p}^2 c_1)^2}{c_1^5 h^2(\tilde{q}_0, \beta)} \quad (14)$$

where $\tilde{q}_0 = \frac{q}{nc_1}$. n_0 is equivalent to the equilibrium density result of Ref. [16] for zero magnetization $\tilde{p} = 0$. We take the limit $q \rightarrow 0$ to obtain a density scale $n_0^{(1)} = \frac{25|c_0|^2}{512\alpha^2 c_1^5}$ and use it to express the dimensionless modified GPE. Since $h(\tilde{q}, \beta)$ is a monotonically increasing function of \tilde{q} , the equilibrium density decrease with the increase of the quadratic Zeeman energy \tilde{q} . Larger \tilde{q} provides stronger BMF fluctuations and the system can stabilize at lower densities.

We use again the locked-in approximation $\Psi(\mathbf{r}) = \psi(\mathbf{r}) \tau^{\text{AF}}$ with $\tau^{\text{AF}} = 1/\sqrt{2}(\sqrt{1+\tilde{p}} \ 0 \ \sqrt{1-\tilde{p}})$ and write the

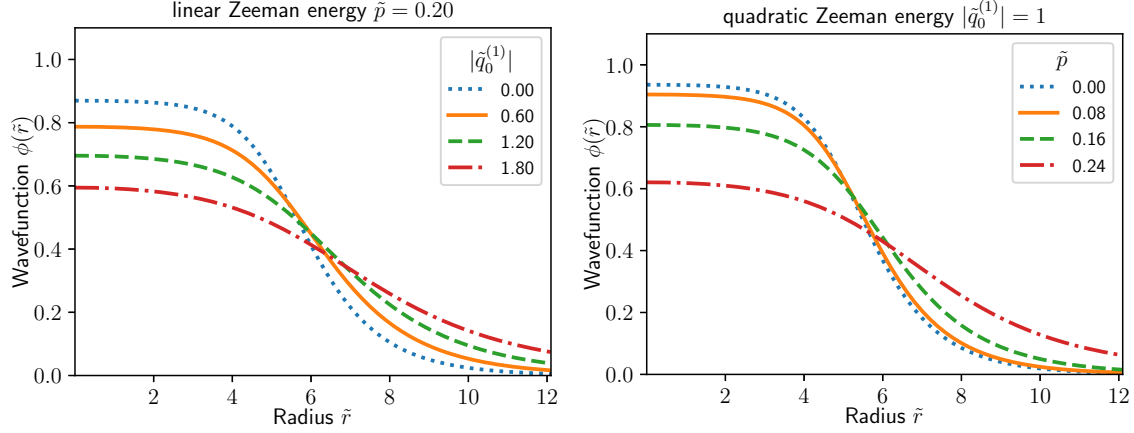


FIG. 4. The ground-state wave functions of the spinor gas in AF phase for various values of quadratic Zeeman $\tilde{q}_0^{(1)}$ and linear Zeeman \tilde{p} energy. The total particle number $\tilde{N} = 500$ and $c_1/c_0 = -5$ with $c_0 < 0$ for both plots. Left: The wave functions for fixed $\tilde{p} = 0.2$ and varying $\tilde{q}_0^{(1)}$. Above \tilde{q}_c , a self-bound droplet cannot be formed. Right: The wave functions for $|\tilde{q}_0^{(1)}| = 1$ and different values of \tilde{p} . Similarly, the above \tilde{p}_c droplet is no longer self-trapped.

energy functional

$$\begin{aligned} \mathcal{E}[\psi^*, \psi] &= \frac{\hbar^2}{2M} |\nabla \psi|^2 + (q - \tilde{p}p) |\psi|^2 + \left(\frac{c_0 + c_1 \tilde{p}^2}{2} \right) |\psi|^4 \\ &+ \frac{8\sqrt{2}}{15} \alpha \{ (c_1 n)^{5/2} I_0(\tilde{q}, \beta) + [(c_0 + c_1)n]^{5/2} I_+(\kappa) \} |\psi|^5. \end{aligned} \quad (15)$$

Using $\psi(\mathbf{r}) = \sqrt{n_0^{(1)}} \phi(\mathbf{r})$, we minimize the total energy $E = \int d^3\mathbf{r} \mathcal{E}[\psi^*, \psi] - \mu N$ with the total number of particles $N = \int d^3\mathbf{r} |\psi|^2$ which yields the modified GPE

$$\begin{aligned} \tilde{\mu} \phi &= -\frac{1}{2} \tilde{\nabla}^2 \phi \\ &+ \left\{ -3 \left(1 + \frac{c_1}{c_0} \tilde{p}^2 \right) |\phi|^2 + \frac{5}{4} I_0 \left(\frac{\tilde{q}_0^{(1)}}{|\phi|^2}, \beta \right) |\phi|^3 \right. \\ &\left. + \frac{5}{4} \left(\frac{c_0}{c_1} + 1 \right)^{5/2} I_+(\kappa) |\phi|^3 - \frac{\tilde{q}_0^{(1)}}{2} I'_0 \left(\frac{\tilde{q}_0^{(1)}}{|\phi|^2}, \beta \right) |\phi| \right\} \phi \end{aligned} \quad (16)$$

where $\tilde{q}_0^{(1)} = \frac{q}{n_0^{(1)} c_1}$, $\tilde{\mathbf{r}} = \mathbf{r}/\xi$, and $\xi = \sqrt{\frac{6\hbar^2}{M|c_0|n_0^{(1)}}}$ is the coherence length of the droplet. In the limit $\tilde{p} \rightarrow 0$, we recover the GPE of the unpolarized AF gas $\tau^{\text{AF}} = 1/\sqrt{2}(1 \ 0 \ 1)$ with $I_+(\kappa) \rightarrow (\frac{c_1}{c_0+c_1})^{5/2}$, which is expected to give a droplet phase up to a critical $|\tilde{q}| \approx 4.4$ for $\tilde{N} \approx 500$ and $c_1/c_0 = -5$ [16].

When $|\tilde{p}| \geq \sqrt{|c_0|/c_1} \approx 0.45$, the blue dashed line in Fig. 3, MF interaction becomes repulsive, the gas goes through expansion, and BMF fluctuations provide corrections for further repulsion. When $|\tilde{p}| < \sqrt{|c_0|/c_1}$ the MF drives a density collapse while BMF interactions are still effectively repulsive. Typically, the effect of \tilde{p} is much more pronounced in the MF terms than the BMF corrections whereas the effect of $|\tilde{q}|$ is small in MF interactions, but it strengthens the BMF fluctuations for given \tilde{p} .

We display the droplet wave functions obtained from the numerical solution of modified GPE for $|\tilde{q}_0^{(1)}| = 1$ with varying \tilde{p} on the right, and for $\tilde{p} = 0.2$ with varying $|\tilde{q}_0^{(1)}|$ on the left panel of Fig. 4.

For a fixed \tilde{p} , larger $|\tilde{q}_0^{(1)}|$ gives stronger BMF repulsion, which widens the droplet radius. For $\tilde{p} = 0.2$, after $|\tilde{q}_c| \approx 2.2$, the gas cannot form a droplet. For a fixed $|\tilde{q}_0^{(1)}|$, greater magnetization \tilde{p} means both lower MF attraction and lower BMF repulsion. Since the polarization changes the MF attraction in a greater ratio than the BMF repulsion, the critical $|\tilde{q}_c|$ becomes lower for greater \tilde{p} . For $\tilde{p} > \tilde{p}_c$ even a small BMF repulsion is sufficient to expand the gas, since the MF attraction becomes much weaker. For instance, after a critical level of $\tilde{p}_c \approx 0.3$ for $|\tilde{q}_0^{(1)}| = 1$, the gas cannot bind into a droplet.

We obtain the critical levels for each $\tilde{q}_0^{(1)}$ and \tilde{p} within the parameter region of interest for $c_1/c_0 = -5$ and show the droplet phase boundary in Fig. 3 with the solid red curve.

VI. DISCUSSION OF EXPERIMENTAL REALIZATION AND CONCLUSION

The parameters of the phase diagrams discussed above are within the current experimental capabilities for the Rabi-coupled gas. Consider a mixture of ^{39}K atoms in the hyperfine states $|F=1, m_F=0\rangle$ and $|F=1, m_F=-1\rangle$. The Feshbach resonance around $B \approx 54.5$ G can be used to tune the intracomponent scattering lengths as $a_{11} = a_{22} = 40a_B$ and the intercomponent scattering length $a_{12} = -60a_B$ [8], where a_B is the Bohr radius. The ratio of interactions gives $\gamma = \frac{g}{g_{12}} = -1.5$. In the absence of detuning and Rabi coupling, $N \approx 23\,000$ particles give a droplet of radius $0.4 \mu\text{m}$ with a peak density $n_0 = 4.12 \times 10^{16} \text{ cm}^{-3}$. For zero detuning $\delta = 0$, one can introduce a Rabi coupling $\omega_R = 2\pi f_R$ up to the level $f_R \approx 51$ kHz. As the Rabi coupling frequency increases, the droplet expands to a radius $r \approx 0.65 \mu\text{m}$ and the density at the center of the droplet decreases to $n_0 \approx 0.8 \times 10^{16} \text{ cm}^{-3}$. Above 51 kHz, the droplet will not be self-bound. The role of nonzero detuning can be tested by setting the Rabi frequency to $f_R = 10.2$ kHz for the same number of particles.

The critical level of detuning for these parameters is $\delta_c = 41$ kHz, which gives density $n_0 = 3.75 \times 10^{16} \text{ cm}^{-3}$ and radius $7.4 \mu\text{m}$ beyond which it is no longer self-bound.

Experimentally realized spinor BECs so far are not favorable for obtaining a spinor droplet since they are all mechanically stable $c_0 > 0$ [28,30–33]. While the use of Feshbach resonance is not possible, the spinor BEC scattering lengths may be tuned using theoretically proposed optical Feshbach resonances in future cold atom settings [34,35]. The scattering lengths that favor droplet formation can be estimated considering an atom with scattering lengths $a_0 = -50a_B$ in the spin-zero channel and $a_2 = 20a_B$ in the spin-1 channel with Landé factor $g_L = 1/2$ ($s = 1/2, l = 0, I = 3/2$) which gives $c_1/c_0 = -5$ with $c_0 < 0$. For zero linear and quadratic Zeeman energies, the spinor droplet with a density $8.3 \times 10^{16} \text{ cm}^{-3}$ and radius $0.6 \mu\text{m}$ can be formed with the total particle number $N \approx 130\,000$. This droplet will be self-bound until a critical level of quadratic Zeeman energy $q \approx 680$ kHz. For an initial magnetization per particle $\tilde{p} = 0.2$, the gas will be stable until the quadratic Zeeman energy exceeds 320 kHz where the density of the droplet at its center will be around $2.1 \times 10^{16} \text{ cm}^{-3}$ and the radius $0.95 \mu\text{m}$.

In conclusion, Rabi-coupled Bose mixture and spinor gas are similar to each other in the following ways.

(i) The BMF energies are Rabi frequency or quadratic Zeeman energy dependent.

(ii) One of the Bogoliubov modes become gapped when nonzero Rabi frequency or quadratic Zeeman energy is introduced.

(iii) The polarization, hence the effective mean-field energy, can be significantly changed using the detuning or linear Zeeman energy.

Therefore, droplet formation and its properties are highly affected by the linear and quadratic Zeeman energies in spinor gases, the Rabi frequency, and the detuning in the Bose mixtures.

Note added. Recently, we became aware of a recent study [36] related to polarized Rabi-coupled Bose mixture.

ACKNOWLEDGMENT

This work is supported by TUBITAK 2236 Co-funded Brain Circulation Scheme 2 (CoCirculation2) Project No. 120C066 (A.K.).

APPENDIX A: THE BOGOLIUBOV THEORY OF RABI-COUPLED MIXTURE

We obtain the MF energy and BMF fluctuations using the Bogoliubov theory in the Hamiltonian (1). Assuming a

homogeneous gas, we express the field operators in terms of Fourier modes $\hat{\Psi}_m(\mathbf{x}) = V^{-1/2} \sum_{\mathbf{k}} \hat{a}_{\mathbf{k},m} e^{i\mathbf{k}\mathbf{x}}$, and write the operators $\hat{a}_{\mathbf{k},m} = \hat{a}_{0,m} + \sum_{\mathbf{k} \neq 0} \hat{a}_{\mathbf{k},m}$ keeping only the terms up to the quadratic order in $\hat{a}_{\mathbf{k} \neq 0, m}$. We replace the operators with the classical number $\hat{a}_{0,m} \approx \sqrt{N_{0,m}}$, where $N_{0,m}$ is the number of particles with internal state m in the $\mathbf{k} = 0$ state. The Hamiltonian (1) becomes

$$\begin{aligned} \hat{H} = & -2\hbar\omega_R\sqrt{N_1N_2} - \frac{\hbar\delta}{2}(N_2 - N_1) + \sum_{m,m'} \frac{g_{mm'}N_mN_{m'}}{2V} \\ & + \sum_{\mathbf{k} \neq 0} \left\{ \left(\epsilon_{\mathbf{k}} + g_{11}n_1 + \hbar\omega_R\sqrt{\frac{N_2}{N_1}} \right) \hat{a}_{\mathbf{k},1}^\dagger \hat{a}_{\mathbf{k},1} \right. \\ & + \left(\epsilon_{\mathbf{k}} + g_{22}n_2 + \hbar\omega_R\sqrt{\frac{N_1}{N_2}} \right) \hat{a}_{\mathbf{k},2}^\dagger \hat{a}_{\mathbf{k},2} \\ & + \frac{g_{11}n_1}{2} (\hat{a}_{\mathbf{k},1}^\dagger \hat{a}_{-\mathbf{k},1}^\dagger + \hat{a}_{\mathbf{k},1} \hat{a}_{-\mathbf{k},1}) \\ & + \frac{g_{22}n_2}{2} (\hat{a}_{\mathbf{k},2}^\dagger \hat{a}_{-\mathbf{k},2}^\dagger + \hat{a}_{\mathbf{k},2} \hat{a}_{-\mathbf{k},2}) \\ & + g_{12}\sqrt{n_1n_2} (\hat{a}_{\mathbf{k},1}^\dagger \hat{a}_{-\mathbf{k},2}^\dagger + \hat{a}_{\mathbf{k},1} \hat{a}_{-\mathbf{k},2}) \\ & \left. + (g_{12}\sqrt{n_1n_2} - \hbar\omega_R) (\hat{a}_{\mathbf{k},1}^\dagger \hat{a}_{\mathbf{k},2} + \hat{a}_{\mathbf{k},2}^\dagger \hat{a}_{\mathbf{k},1}) \right\} \quad (\text{A1}) \end{aligned}$$

where $\epsilon_{\mathbf{k}} = \frac{\hbar^2 k^2}{2M}$ is the free particle dispersion. The first line of (A1) is the MF energy of the Rabi-coupled binary mixture gas, while the rest of the terms account for the quantum fluctuations that constitute the BMF energy.

The MF energy of Rabi-coupled gas reads

$$E_{\text{MF}} = -2\hbar\omega_R\sqrt{N_1N_2} - \frac{\hbar\delta}{2}(N_2 - N_1) + \sum_{m,m'} \frac{g_{mm'}N_mN_{m'}}{2V}. \quad (\text{A2})$$

For equal intraspecies coupling $g_{11} = g_{22} = g$ and the parametrization of particle number ratio of the components with $\tan(\theta/2) = N_1/N_2$ and $N_1 + N_2 = N$, the MF energy in (A2) becomes

$$\frac{E_{\text{MF}}}{N} = -\hbar\omega_R \sin \theta - \frac{\hbar\delta}{2} \cos \theta + \frac{gN}{2V} - \frac{\bar{g}N}{2V} \sin^2 \theta. \quad (\text{A3})$$

By applying the Bogoliubov transformation on the quadratic Hamiltonian (A1), the Bogoliubov modes of the Rabi-coupled binary mixture [24] are obtained:

$$\begin{aligned} E_{\pm, \mathbf{k}} = & \sqrt{D_{\mathbf{k}} \pm \sqrt{D_{\mathbf{k}}^2 - \epsilon_{\mathbf{k}} \left(\epsilon_{\mathbf{k}} + \hbar\omega_R \left(r + \frac{1}{r} \right) \right) \left[\left(\epsilon_{\mathbf{k}} + 2gn_1 + \hbar\omega_R \frac{1}{r} \right) \left(\epsilon_{\mathbf{k}} + 2gn_2 + \hbar\omega_R r \right) - (2g_{12}\sqrt{n_1n_2} - \hbar\omega_R)^2 \right]}}, \\ D_{\mathbf{k}} = & \frac{1}{2} \sum_{m=1,2} \left[\left(\epsilon_{\mathbf{k}} + \hbar\omega_R \sqrt{\frac{n_{\bar{m}}}{n_m}} \right) \left(\epsilon_{\mathbf{k}} + 2gn_m + \hbar\omega_R \sqrt{\frac{n_{\bar{m}}}{n_m}} \right) - \hbar\omega_R (2g_{12}\sqrt{n_1n_2} - \hbar\omega_R) \right] \quad (\text{A4}) \end{aligned}$$

where $\bar{m} = 3 - m$, $n_1 = \frac{r^2}{r^2+1}n$, and $n_2 = \frac{1}{r^2+1}n$. These Bogoliubov modes reduce to the results of Cappellaro *et al.* [8] for $r = 1$ and nonzero ω_R , and they recover the usual Bose mixture results without Rabi coupling for $\omega_R = 0$ and $r = 1$.

The total BMF energy is the zero-point energy of the Bogoliubov excitations:

$$E_{\text{BMF}} = \frac{1}{2} \sum_{\mathbf{k}} \left\{ E_{+, \mathbf{k}} + E_{-, \mathbf{k}} - 2\epsilon_{\mathbf{k}} - \left(r + \frac{1}{r} \right) \hbar\omega_R - gn_1 - gn_2 + \frac{g^2 n_1^2 + g^2 n_2^2 + 2g_{12}^2 n_1 n_2}{2\epsilon_{\mathbf{k}}} \right\} \quad (\text{A5})$$

where the last term within the summation is the T-matrix renormalization energy for the Bose mixture [2].

To calculate the BMF energy of each mode separately, we divide the renormalization energy among the two modes such that none of the modes yield divergence. We calculate each corresponding Bogoliubov mode separately using $E_{\text{BMF}}^{\pm} = \frac{1}{2} \sum_{\mathbf{k}} (E_{\mathbf{k}}^{\pm} - \lim_{\mathbf{k} \rightarrow \infty} E_{\mathbf{k}}^{\pm})$, which gives

$$\frac{E_{\text{BMF}}^{\pm}}{V} = \alpha (gn)^{5/2} I_{\pm}(\tilde{\omega}, \gamma, r) \quad (\text{A6})$$

where $\alpha = \frac{M^{3/2}}{\sqrt{2\pi^2 \hbar^3}}$, $\tilde{\omega} = \frac{\hbar\omega_R}{gn}$, the particle number ratio $r = \sqrt{\frac{N_1}{N_2}}$, and coupling constant ratio $\gamma = \frac{g_{12}}{g}$.

The integral expression for the function $I_{\pm}(\tilde{\omega}, r, \gamma)$ within the BMF energy (A6) is given by

$$I_{\pm}(\tilde{\omega}, \gamma, r) \equiv \left(\frac{r^2}{r^2+1} \right)^{5/2} \int_0^{\infty} dy y^2 \left\{ \sqrt{(y^4 + \beta_2 y^2 + \beta_0) \pm \sqrt{(\beta_2^2 + 2\beta_0 - z_4)y^4 + (2\beta_0\beta_2 - z_6)y^2 + \beta_0^2}} \right. \\ \left. - y^2 \left[1 + \frac{\beta_2 \pm \sqrt{\beta_2^2 + 2\beta_0 - z_4}}{2y^2} + \frac{\beta_0 \pm \frac{\beta_0\beta_2 - z_6/2}{\sqrt{\beta_2^2 + 2\beta_0 - z_4}} - \frac{(\beta_2 \pm \sqrt{\beta_2^2 + 2\beta_0 - z_4})^2}{4}}{2y^4} \right] \right\} \quad (\text{A7})$$

where

$$\beta_0 \equiv \frac{(r^2+1)^2}{r^4} \left[\frac{2r\tilde{\omega}}{r^2+1}(1-\gamma) + \tilde{\omega}^2 + \frac{\tilde{\omega}^2}{2r^2} + \frac{\tilde{\omega}^2 r^2}{2} \right], \quad (\text{A8})$$

$$\beta_2 \equiv \left(1 + \frac{1}{r^2} \right) \left(1 + \frac{\tilde{\omega}}{r} + \tilde{\omega}r \right), \quad (\text{A9})$$

$$z_4 \equiv \left(2 + \frac{\tilde{\omega}(r^2+1)}{r^3} \right) \left(\frac{2}{r^2} + \frac{\tilde{\omega}(r^2+1)}{r} \right) + \tilde{\omega} \frac{(r^2+1)^3}{r^5} \left(2 + \frac{\tilde{\omega}(r^2+1)}{r} \right) - \left(\frac{2\gamma}{r} - \frac{\tilde{\omega}(r^2+1)}{r^2} \right)^2, \quad (\text{A10})$$

$$z_6 \equiv \tilde{\omega} \frac{(r^2+1)^2}{r^3} \left[\left(2 + \frac{\tilde{\omega}(r^2+1)}{r^3} \right) \left(\frac{2}{r^2} + \frac{\tilde{\omega}(r^2+1)}{r} \right) - \left(\frac{2\gamma}{r} - \frac{\tilde{\omega}(r^2+1)}{r^2} \right)^2 \right] \quad (\text{A11})$$

where $gn_1 y^2 \equiv \epsilon_{\mathbf{k}}$. Check Fig. 5 to see how $I_+(\tilde{\omega}, \gamma, r)$ behaves for various r values as $\tilde{\omega}$ changes.

APPENDIX B: BOGOLIUBOV THEORY OF SPIN-1 GAS

With the Bogoliubov approximation, the Hamiltonian in (9) reduces to quadratic form [37]:

$$\hat{H}_{\text{eff}} = \frac{Vn^2}{2} (c_0 + c_1 \langle \mathbf{F} \rangle^2) + qN \langle F_z^2 \rangle - pN \langle F_z \rangle \\ + \sum_{\mathbf{k} \neq 0} \left\{ [\epsilon_{\mathbf{k}} - nc_1 \langle \mathbf{F} \rangle^2 + qm^2 - q \langle F_z^2 \rangle] \hat{a}_{\mathbf{k}, m}^{\dagger} \hat{a}_{\mathbf{k}, m} \right. \\ + nc_1 \langle \mathbf{F} \rangle \cdot \mathbf{F}_{m m'} \hat{a}_{\mathbf{k}, m}^{\dagger} \hat{a}_{\mathbf{k}, m'} \\ + \frac{nc_0}{2} (2\hat{D}_{\mathbf{k}}^{\dagger} \hat{D}_{\mathbf{k}} + \hat{D}_{\mathbf{k}} \hat{D}_{-\mathbf{k}} + \hat{D}_{\mathbf{k}}^{\dagger} \hat{D}_{-\mathbf{k}}^{\dagger}) \\ \left. + \frac{nc_1}{2} (2\hat{\mathbf{F}}_{\mathbf{k}}^{\dagger} \hat{\mathbf{F}}_{\mathbf{k}} + \hat{\mathbf{F}}_{\mathbf{k}} \hat{\mathbf{F}}_{-\mathbf{k}} + \hat{\mathbf{F}}_{\mathbf{k}}^{\dagger} \hat{\mathbf{F}}_{-\mathbf{k}}^{\dagger}) \right\} \quad (\text{B1})$$

where $\epsilon_{\mathbf{k}} = \hbar^2 \mathbf{k}^2 / 2M$ is the free particle dispersion, $\langle \mathbf{F} \rangle \equiv \sum_{m, m'} \mathbf{F}_{m m'} \tau_m^* \tau_{m'}$ is the expectation value of the spin-1 order parameter, $\hat{D}_{\mathbf{k}} \equiv \sum_m \tau_m^* \hat{a}_{\mathbf{k}, m}$ and $\hat{\mathbf{F}}_{\mathbf{k}} \equiv \sum_{m, m'} \mathbf{F}_{m m'} \tau_m^* \hat{a}_{\mathbf{k}, m'}$ are the density and spin fluctuation operators, N_0 is the number of particles in the $\mathbf{k} = 0$ state, and τ is the ground-state order parameter in the spin-1 manifold.

The MF energy of the spin-1 BEC obtained from (B1) is [37]

$$\frac{E_{\text{MF}}}{V} = \frac{n^2}{2} (c_0 + c_1 \langle \mathbf{F} \rangle^2) + qn \langle F_z^2 \rangle - pn \langle F_z \rangle \quad (\text{B2})$$

whereas all the other terms within the summation constitute the quantum fluctuations.

The order parameter τ_{AF} gives $\langle F_z^2 \rangle = 1$, $\langle F_z \rangle = \bar{p}$, and $\langle \mathbf{F} \rangle = \bar{p} \hat{e}_z$ and the resulting quadratic Hamiltonian is

$$\hat{H} = E_0^{\text{AF}} + \sum_{\mathbf{k} \neq 0} \left\{ (\epsilon_{\mathbf{k}} - q + c_1 n) \hat{a}_{\mathbf{k}, 0}^{\dagger} \hat{a}_{\mathbf{k}, 0} \right. \\ \left. + \frac{c_1 n \beta}{2} (\hat{a}_{\mathbf{k}, 0}^{\dagger} \hat{a}_{-\mathbf{k}, 0}^{\dagger} + \hat{a}_{\mathbf{k}, 0} \hat{a}_{-\mathbf{k}, 0}) \right\}$$

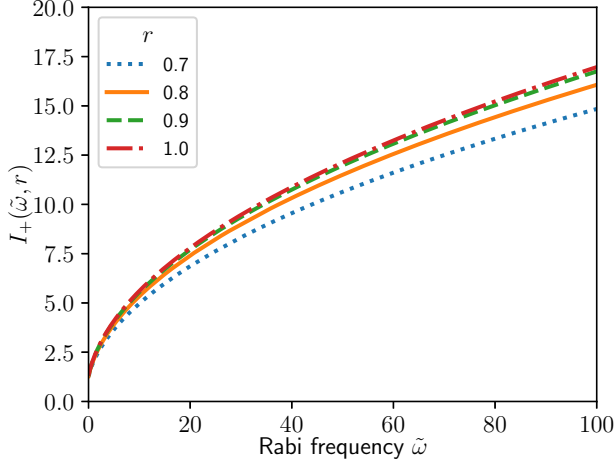


FIG. 5. The integral I_+ in (A7) as a function $\tilde{\omega}$ for various r and fixed $g_{12}/g = -1.5$.

$$\begin{aligned}
& + \sum_{m=\pm 1} \left[\epsilon_{\mathbf{k}} + \frac{(c_0 + c_1)n(1 + m\tilde{p})}{2} \right] \hat{a}_{\mathbf{k},m}^\dagger \hat{a}_{\mathbf{k},m} \\
& + \sum_{m=\pm 1} \left[\frac{(c_0 + c_1)n(1 + m\tilde{p})}{4} \right] (\hat{a}_{\mathbf{k},m}^\dagger \hat{a}_{-\mathbf{k},m}^\dagger + \hat{a}_{\mathbf{k},m} \hat{a}_{-\mathbf{k},m}) \\
& + \frac{(c_0 - c_1)n\beta}{4} (2\hat{a}_{\mathbf{k},-1}^\dagger \hat{a}_{\mathbf{k},1} + \hat{a}_{\mathbf{k},-1}^\dagger \hat{a}_{-\mathbf{k},1}^\dagger + \hat{a}_{\mathbf{k},1}^\dagger \hat{a}_{-\mathbf{k},-1}^\dagger \\
& + 2\hat{a}_{\mathbf{k},1}^\dagger \hat{a}_{\mathbf{k},-1} + \hat{a}_{\mathbf{k},-1} \hat{a}_{-\mathbf{k},1} + \hat{a}_{\mathbf{k},1} \hat{a}_{-\mathbf{k},-1}) \} \quad (\text{B3})
\end{aligned}$$

where $\beta = \sqrt{1 - \tilde{p}^2}$, and E_0^{AF} is the MF energy:

$$\frac{E_0^{\text{AF}}}{V} = (q - \tilde{p}p)n + \frac{(c_0 + c_1\tilde{p}^2)n^2}{2}. \quad (\text{B4})$$

The diagonalization of the quadratic Hamiltonian in (B3) yields three distinct Bogoliubov modes [27]:

$$\begin{aligned}
E_{k,\pm 1} &= \sqrt{\epsilon_{\mathbf{k}}[\epsilon_{\mathbf{k}} + (c_0 + c_1)n(1 \pm \kappa)]}, \\
E_{k,0} &= \sqrt{(\epsilon_{\mathbf{k}} - q + (1 - \beta)c_1n)(\epsilon_{\mathbf{k}} - q + (1 + \beta)c_1n)} \quad (\text{B5})
\end{aligned}$$

where $\kappa \equiv \sqrt{1 - \frac{4\beta^2 c_0 c_1}{(c_0 + c_1)^2}}$. To calculate the renormalization terms, rewrite the two-body interaction energy in the MF energy functional (B4) as

$$\frac{(c_0 + c_1\tilde{p}^2)n^2}{2} = \frac{[\tilde{p}^2(c_0 + c_1) + (1 - \tilde{p}^2)c_0]n^2}{2}. \quad (\text{B6})$$

Then, replace the bare coupling constants c_0 and $c_0 + c_1$ in (B6) with the renormalized coupling constants \bar{c}_0 and $\bar{c}_0 + \bar{c}_1$ by using the T-matrix approach up to the second order (see the Appendix of Ref. [37]):

$$\bar{c}_0 = c_0 + \frac{(c_0^2 + 2c_1^2)}{V} \sum_{\mathbf{k} \neq 0} \frac{1}{2\epsilon_{\mathbf{k}}}, \quad (\text{B7})$$

$$\bar{c}_0 + \bar{c}_1 = (c_0 + c_1) + \frac{(c_0 + c_1)^2}{V} \sum_{\mathbf{k} \neq 0} \frac{1}{2\epsilon_{\mathbf{k}}}. \quad (\text{B8})$$

Then, we distribute the total renormalization energy into three distinct modes to avoid the divergence in each mode separately. The BMF energies become

$$\begin{aligned}
E_{\text{BMF},\pm 1} &= \frac{1}{2} \sum_{\mathbf{k} \neq 0} \left\{ E_{k,\pm 1} - \left(\epsilon_{\mathbf{k}} + \frac{(c_0 + c_1)(1 \pm \tilde{p})n}{2} \right) \right. \\
&\quad \left. + \frac{(\kappa^2 + 1)(c_0 + c_1)^2 n^2}{4\epsilon_{\mathbf{k}}} \right\}, \quad (\text{B9})
\end{aligned}$$

$$\begin{aligned}
E_{\text{BMF},0} &= \frac{1}{2} \sum_{\mathbf{k} \neq 0} \left\{ E_{k,0} - (\epsilon_{\mathbf{k}} - \tilde{q} + c_1n) + \frac{\beta^2(c_1n)^2}{2\epsilon_{\mathbf{k}}} \right\} \quad (\text{B10})
\end{aligned}$$

where $\tilde{q} = \frac{q}{nc_1}$. Then, we obtain the following total BMF energy density for the AF order parameter:

$$\begin{aligned}
\frac{E_{\text{BMF}}^{\text{AF}}}{V} &= \frac{8\sqrt{2}}{15} \alpha (c_1n)^{5/2} I_0(\tilde{q}, \beta) \\
&\quad + \frac{8\sqrt{2}}{15} \alpha [(c_0 + c_1)n]^{5/2} [I_+(\kappa) + I_-(\kappa)] \quad (\text{B11})
\end{aligned}$$

where $I_{\pm} = \frac{(1 \pm \kappa)^{5/2}}{4\sqrt{2}}$ and $I_0(\tilde{q}, \beta)$ can be approximated as (see Appendix C)

$$I_0(\tilde{q}, \beta) \approx \frac{15\pi\beta^2}{32\sqrt{2}} \left[\sqrt{-\tilde{q} + 1} - \frac{\beta^2}{32} \frac{1}{(-\tilde{q} + 1)^{3/2}} \right]. \quad (\text{B12})$$

APPENDIX C: ANALYTICAL APPROXIMATION FOR $I_0(\tilde{q}, \beta)$

The integral that determines the BMF energy for the $E_{k,0}$ mode reads

$$\begin{aligned}
I_0(\tilde{q}, \beta) &= \frac{15}{8\sqrt{2}} \int_0^\infty dx x^2 \\
&\quad \times \left[\sqrt{(x^2 - \tilde{q} + 1)^2 - \beta^2} - (x^2 - \tilde{q} + 1) + \frac{\beta^2}{2x^2} \right] \quad (\text{C1})
\end{aligned}$$

where $\epsilon_{\mathbf{k}} \equiv c_1 n x^2$ substitution is done.

We use a change of variable $y \equiv x^2 - \tilde{q} + 1$ in the integral (C1) and expand $\sqrt{1 - \beta^2/y^2}$ in Taylor series up to the second order in the domain $x \geq 0$ and $\tilde{q} \leq 0$ and obtain

$$\begin{aligned}
I_0(\tilde{q}, \beta) &= -\frac{15\beta^2}{16\sqrt{2}} \int_0^\infty dx \left(\frac{(\tilde{q} - 1)}{x^2 - \tilde{q} + 1} + \frac{\beta^2 x^2}{4(x^2 - \tilde{q} + 1)^3} \right). \quad (\text{C2})
\end{aligned}$$

Each term above can be calculated to give

$$I_0(\tilde{q}, \beta) \approx \frac{15\pi\beta^2}{32\sqrt{2}} \left[\sqrt{-\tilde{q} + 1} - \frac{\beta^2}{32} \frac{1}{(-\tilde{q} + 1)^{3/2}} \right]. \quad (\text{C3})$$

Higher-order terms in the expansion of $\sqrt{1 - \beta^2/y^2}$ improve the accuracy but we numerically checked that the second-order expansion is sufficient to achieve less than 1% error for all \tilde{q} values.

- [1] F. Wächtler and L. Santos, Ground-state properties and elementary excitations of quantum droplets in dipolar Bose-Einstein condensates, *Phys. Rev. A* **94**, 043618 (2016).
- [2] D. S. Petrov, Quantum Mechanical Stabilization of a Collapsing Bose-Bose Mixture, *Phys. Rev. Lett.* **115**, 155302 (2015).
- [3] C. J. Pethick and H. Smith, *Bose-Einstein Condensation in Dilute Gases* (Cambridge University, New York, 2008).
- [4] I. Ferrier-Barbut, H. Kadau, M. Schmitt, M. Wenzel, and T. Pfau, Observation of Quantum Droplets in a Strongly Dipolar Bose Gas, *Phys. Rev. Lett.* **116**, 215301 (2016).
- [5] M. Schmitt, M. Wenzel, F. Böttcher, I. Ferrier-Barbut, and T. Pfau, Self-bound droplets of a dilute magnetic quantum liquid, *Nature (London)* **539**, 259 (2016).
- [6] A. Macia, J. Sánchez-Baena, J. Boronat, and F. Mazzanti, Droplets of Trapped Quantum Dipolar Bosons, *Phys. Rev. Lett.* **117**, 205301 (2016).
- [7] D. Baillie, R. M. Wilson, R. N. Bisset, and P. B. Blakie, Self-bound dipolar droplet: A localized matter wave in free space, *Phys. Rev. A* **94**, 021602(R) (2016).
- [8] A. Cappellaro, T. Macrì, G. F. Bertacco, and L. Salasnich, Equation of state and self-bound droplet in Rabi-coupled Bose mixtures, *Sci. Rep.* **7**, 13358 (2017).
- [9] C. R. Cabrera, L. Tanzi, J. Sanz, B. Naylor, P. Thomas, P. Cheiney, and L. Tarruell, Quantum liquid droplets in a mixture of Bose-Einstein condensates, *Science* **359**, 301 (2018).
- [10] G. Semeghini, G. Ferioli, L. Masi, C. Mazzinghi, L. Wolswijk, F. Minardi, M. Modugno, G. Modugno, M. Inguscio, and M. Fattori, Self-Bound Quantum Droplets of Atomic Mixtures in Free Space, *Phys. Rev. Lett.* **120**, 235301 (2018).
- [11] E. Aybar and M. O. Oktel, Temperature-dependent density profiles of dipolar droplets, *Phys. Rev. A* **99**, 013620 (2019).
- [12] J. Sánchez-Baena, J. Boronat, and F. Mazzanti, Supersolid striped droplets in a Raman spin-orbit-coupled system, *Phys. Rev. A* **102**, 053308 (2020).
- [13] K. E. Wilson, A. Guttridge, J. Segal, and S. L. Cornish, Quantum degenerate mixtures of Cs and Yb, *Phys. Rev. A* **103**, 033306 (2021).
- [14] Y. Ma, C. Peng, and X. Cui, Borromean Droplet in Three-Component Ultracold Bose Gases, *Phys. Rev. Lett.* **127**, 043002 (2021).
- [15] R. N. Bisset, L. A. Peña Ardila, and L. Santos, Quantum Droplets of Dipolar Mixtures, *Phys. Rev. Lett.* **126**, 025301 (2021).
- [16] T. A. Yoğurt, A. Keleş, and M. O. Oktel, Spinor boson droplets stabilized by spin fluctuations, *Phys. Rev. A* **105**, 043309 (2022).
- [17] F. Böttcher, M. Wenzel, J.-N. Schmidt, M. Guo, T. Langen, I. Ferrier-Barbut, T. Pfau, R. Bombín, J. Sánchez-Baena, J. Boronat *et al.*, Dilute dipolar quantum droplets beyond the extended Gross-Pitaevskii equation, *Phys. Rev. Res.* **1**, 033088 (2019).
- [18] Q. Gu and L. Yin, Phonon stability and sound velocity of quantum droplets in a boson mixture, *Phys. Rev. B* **102**, 220503(R) (2020).
- [19] M. Ota and G. Astrakharchik, Beyond Lee-Huang-Yang description of self-bound Bose mixtures, *SciPost Phys.* **9**, 020 (2020).
- [20] H. Hu and X.-J. Liu, Consistent Theory of Self-Bound Quantum Droplets with Bosonic Pairing, *Phys. Rev. Lett.* **125**, 195302 (2020).
- [21] R. Oldziejewski and K. Jachymski, Properties of strongly dipolar Bose gases beyond the Born approximation, *Phys. Rev. A* **94**, 063638 (2016).
- [22] Y. Wang, L. Guo, S. Yi, and T. Shi, Theory for self-bound states of dipolar Bose-Einstein condensates, *Phys. Rev. Res.* **2**, 043074 (2020).
- [23] E. Chiquillo, Low-dimensional self-bound quantum Rabi-coupled bosonic droplets, *Phys. Rev. A* **99**, 051601(R) (2019).
- [24] L. Lavoine, A. Hammond, A. Recati, D. S. Petrov, and T. Bourdel, Beyond-Mean-Field Effects in Rabi-Coupled Two-Component Bose-Einstein Condensate, *Phys. Rev. Lett.* **127**, 203402 (2021).
- [25] A. Hammond, L. Lavoine, and T. Bourdel, Tunable Three-Body Interactions in Driven Two-Component Bose-Einstein Condensates, *Phys. Rev. Lett.* **128**, 083401 (2022).
- [26] M. Abad and A. Recati, A study of coherently coupled two-component Bose-Einstein condensates, *Eur. Phys. J. D* **67**, 148 (2013).
- [27] Y. Kawaguchi and M. Ueda, Spinor Bose-Einstein condensates, *Phys. Rep.* **520**, 253 (2012).
- [28] D. M. Stamper-Kurn and M. Ueda, Spinor Bose gases: Symmetries, magnetism, and quantum dynamics, *Rev. Mod. Phys.* **85**, 1191 (2013).
- [29] J. Guzman, G.-B. Jo, A. N. Wenz, K. W. Murch, C. K. Thomas, and D. M. Stamper-Kurn, Long-time-scale dynamics of spin textures in a degenerate $F = 1$ ^{87}Rb spinor Bose gas, *Phys. Rev. A* **84**, 063625 (2011).
- [30] J. Stenger, S. Inouye, D. M. Stamper-Kurn, H.-J. Miesner, A. P. Chikkatur, and W. Ketterle, Spin domains in ground-state Bose-Einstein condensates, *Nature (London)* **396**, 345 (1998).
- [31] M.-S. Chang, C. D. Hamley, M. D. Barrett, J. A. Sauer, K. M. Fortier, W. Zhang, L. You, and M. S. Chapman, Observation of Spinor Dynamics in Optically Trapped ^{87}Rb Bose-Einstein condensates, *Phys. Rev. Lett.* **92**, 140403 (2004).
- [32] A. T. Black, E. Gomez, L. D. Turner, S. Jung, and P. D. Lett, Spinor Dynamics in an Antiferromagnetic Spin-1 Condensate, *Phys. Rev. Lett.* **99**, 070403 (2007).
- [33] S. J. Huh, K. Kim, K. Kwon, and J. Y. Choi, Observation of a strongly ferromagnetic spinor Bose-Einstein condensate, *Phys. Rev. Res.* **2**, 033471 (2020).
- [34] T. L. Nicholson, S. Blatt, B. J. Bloom, J. R. Williams, J. W. Thomsen, J. Ye, and P. S. Julienne, Optical Feshbach resonances: Field-dressed theory and comparison with experiments, *Phys. Rev. A* **92**, 022709 (2015).
- [35] O. Thomas, C. Lippe, T. Eichert, and H. Ott, Experimental realization of a Rydberg optical Feshbach resonance in a quantum many-body system, *Nat. Commun.* **9**, 2238 (2018).
- [36] Q. Gu and X. Cui, Liquid-gas coexistence in binary Bose-Einstein condensates, [arXiv:2209.10019](https://arxiv.org/abs/2209.10019).
- [37] S. Uchino, M. Kobayashi, and M. Ueda, Bogoliubov theory and Lee-Huang-Yang corrections in spin-1 and spin-2 Bose-Einstein condensates in the presence of the quadratic Zeeman effect, *Phys. Rev. A* **81**, 063632 (2010).